Mechanical Systems and Signal Processing 24 (2010) 2844–2854

Contents lists available at ScienceDirect

Mechanical Systems and Signal Processing

journal homepage: www.elsevier.com/locate/jnlabr/ymssp

Nonlinear model identification of a frictional contact support

Hamid Ahmadian*, Hassan Jalali, Fatemeh Pourahmadian

Center of Excellence in Solid Mechanics and Dynamics, Iran University of Science and Technology, Narmak, Tehran, Iran

ARTICLE INFO

Article history:
Received 11 November 2009
Received in revised form
3 June 2010
Accepted 22 June 2010
Available online 26 June 2010

Keywords:
Frictional support
Nonlinear normal mode
Force state mapping

ABSTRACT

Accurate predictions of a structure dynamics require precise modeling of its boundary conditions including any nonlinear effects. This paper investigates the behavior of frictional supports that are examples of boundary conditions exhibiting nonlinear effects, such as stiction and slip phenomena, depending on the structure vibration amplitudes. The dependency of restoring forces in a frictional contact to the vibration amplitude level is identified in this study using experimental observations. In an experimental case study measured responses of a beam fixed at one end and frictionally supported at the other end were expanded using corresponding nonlinear normal modes of the structure and a reduced order model of the continuous system containing dominant nonlinear effects of the contact was obtained. The obtained discrete model constitutes bases for identification of restoring forces in the contact interface using force state mapping. The identified nonlinear restoring forces are then employed to specify parameters of a predictive contact model for the boundary support. The obtained contact model is capable of predicting damping and softening effects due to micro/macro-slippage and accurately regenerates the experimental results at various response levels.

1. Introduction

Dynamic characteristics of mechanical structures are strongly affected by the nature of their boundary conditions. Dynamic response analysis of these structures requires accurate knowledge of the mechanisms involved in the boundary interfaces and the ability to include them in their models. This issue becomes even more important when nonlinear effects are involved and the dynamic behavior changes nature as the structure response amplitude exceeds certain levels. Frictional contact interfaces are examples of such nonlinear boundary conditions. Under low vibration amplitudes the interface is in stick regime and the structure behaves linearly. As the vibration amplitude increases slippage at the contact interface develops and the structure behaves in a nonlinear manner.

The study of the dynamics of mechanical structures containing frictional interfaces has a long history. Den Hartog [1] was one of the pioneers who studied the steady state response of a mechanical oscillator containing combined Coulomb friction and viscous damping. Dowell [2] has examined the case of damping in the boundary supports of clamped beams and plates, with primary emphasis on the macro-slip in the boundary. Lee and Feng [3] considered the dynamic response analysis of a beam having frictionally contact boundary interfaces. They modeled the frictional force at the joint by employing the Coulomb friction model. Ferri and Bindemann [4] examined the damping in supports of vibrating beams considering a variety of physical configurations (in-plane slip, transverse slip, etc.). They employed the harmonic balance

* Corresponding author. Tel.: +98 21 77491228; fax: +98 21 77240488.
E-mail address: ahmadian@iust.ac.ir (H. Ahmadian).

0888-3270/$ - see front matter © 2010 Elsevier Ltd. All rights reserved.
doi:10.1016/j.ymssp.2010.06.007

method to determine the response to harmonic excitations and in each configuration they found the friction damping was related to the response amplitude in a different manner, i.e. invariant, proportional, and inversely proportional.

This paper considers the nonlinear behavior of a beam with frictional contact support. In an experimental case study a constant normal force is applied on the contact interface while the level of the beam response is increased by controlling the excitation force amplitude. This creates different behaviors in the contact interface ranging from sticking to micro-slips and finally macro-slips at higher response levels. The objective is to identify the restoring forces in the frictional contact. The continuous system under consideration is discretized using its nonlinear modes. The friction force is identified in a non-parametric form using force-states mapping technique [18,19]. In the identification procedure no assumptions are made regarding the friction force model, and it is identified in terms of contact states, i.e. the sliding motion at the friction support and its time derivative.

Next an appropriate contact model is selected to simulate the identified nonlinear behavior of the contact to be able to predict the friction forces at vibration levels other than those employed in the identification process. Comprehensive investigation of friction contacts is performed by Ferri [5], Berger [6], and Ibrahim and Pettit [7]. Various models have been proposed over the past years addressing the contact interface mechanisms. Among them are the so called micro-slip models, which allow partial slip in some areas of contact surface. The Iwan model [8] is commonly used to model micro-slips and consists of an array of parallel springs in series with Coulomb friction elements. This model is also referred to as elastic–perfectly plastic model. There are other friction models offering smooth transition from stick to micro-slip and macro-slip (sliding) behavior. The Dahl model [9], the Valanis model [10,11], the Leuven model [12,13] and bristle models [14] are some examples. Bristle models capture both the micro-slip and macro-slip regimes of interfacial friction. The LuGre friction model [15] is also based on a bristle interpretation of the frictional interface. These friction models have been widely used by many researchers in constructing mathematical representation of structures containing frictional interfaces. Gaul and Nitsche [16] and Segalman [17] described a range of constitutive and phenomenological models for joint interface mechanisms.

It is observed the identified hysteresis loops of the frictional support are similar to those predicted by the constitutive elasto-plastic Valanis model [10,11] and the predictive model is capable of simulating the nonlinear characteristics of the contact. Introduction of this predictive model with appropriate parameters enables one to determine the frictional forces at vibration levels other than those employed in the identification of the contact model parameters.

The remainder of this paper is organized as follows. Section 2 presents an analytical model for a fixed-frictionally supported Euler–Bernoulli beam. The nonlinear response of the beam to a harmonic excitation is expanded using its nonlinear modes. As the excitation frequency is close to the first resonance frequency of the beam only a few modes are required to express the nonlinear behavior of the beam. Using the nonlinear modes identified from measured responses, the restoring force and response at the frictional contact are determined. Section 3 describes the experimental setup and the test procedure. Results observed in the experimental procedure are employed in Section 4 to identify the contact frictional force and associated contact model parameters.

2. Mathematical modeling

This paper considers the dynamic behavior of a fixed-frictionally supported beam as shown in Fig. 1. The dynamic behavior of beam is modeled using the Euler–Bernoulli beam theory. The uniform beam with constant properties has a modulus of elasticity E, cross sectional moment of inertia I, mass density ρ, cross section area A, and length L. The structure is excited using a concentrated force $f(t)$ at a distance S measured from its fixed end. A normal constant force F is applied on the frictional support. The applied normal force is large enough to restrict the lateral movement of the beam at frictional support but rotation and axial movements are allowed at this end.

The lateral vibration of the uniform continuous beam is governed using a nonlinear partial differential equation as follows:

$$EI\frac{\partial^4 w}{\partial x^4} - N(t)\frac{\partial^2 w}{\partial x^2} + \rho A\frac{\partial^2 w}{\partial t^2} = f(t)\delta(x-S) - rN(t)\delta'(x-L) \tag{1}$$

The nonlinear effects on the lateral deflection w are included in the system via frictional contact force $N(t)$ at the boundary. There is an offset r between neutral axis of the beam and the frictional force line of action which causes a bending moment at the boundary. This bending moment is applied to the beam model using $\delta'(x)$, which is the spatial

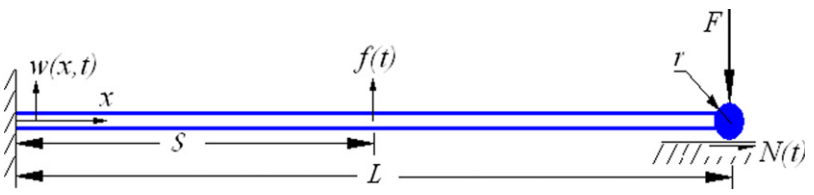

Fig. 1. A slender beam with frictional contact boundary condition.

derivative of the Dirac delta function $\delta(x)$, commonly known as a spatial unit doublet [20]. The axial force $N(t)$ takes into account the linear and nonlinear characteristics of the contact shear forces. The restoring force characteristics include nonlinearities in stiffness and damping and are identified in this paper using experimental observations. In the current modeling axial inertial effects of the beam are neglected as the dynamic behavior of beam is considered in a frequency range much lower than its first axial mode.

In this study, the external excitation force $f(t)$ is a single harmonic force in the vicinity of the first resonance frequency of the structure. As the structure has well separated modes, the mode shapes of its equivalent linearized model at each response amplitude level remain almost real despite the fact that the damping model is non-proportional. Therefore nonlinear behavior of the beam can be spanned using its nonlinear normal modes $\tilde{\varphi}_i(x,a)$; the nonlinear normal modes are real valued functions of the beam maximum response amplitude a at the driving point, i.e.:

$$a = \max w(S,t) \tag{2a}$$

The nonlinear normal modes are equal to the deformed shapes of the corresponding linearized structure at the same response amplitude level [21,22]. Note that the structure has well separated modes and the beam response is expressed using its first n nonlinear normal modes as follows:

$$w(x,t) = \sum_{i=1}^{n} \tilde{\phi}_i(x,a) q_i(t) \tag{2b}$$

Substituting the expansion series described in Eq. (2b) into the nonlinear equation of motions (1) and employing the orthogonality properties of equivalent linearized modes at each response amplitude level a, one arrives at the following discrete equations of motion:

$$\ddot{q}_i + {\omega_i}^2 q_i - f(t)\tilde{\phi}_i(S,a) - k_\theta(a)\frac{\partial\tilde{\phi}_i(L,a)}{\partial x}\sum_{r=1}^{n}\frac{\partial\tilde{\phi}_r(L,a)}{\partial x}q_r(t) = \left(r\frac{\partial\tilde{\phi}_i(L,a)}{\partial x} - \sum_{r=1}^{n} q_r(t)\int_0^L \frac{\partial\tilde{\phi}_i(x,a)}{\partial x}\frac{\partial\tilde{\phi}_r(x,a)}{\partial x}\,dx\right)N(t), \quad i=1,2,\ldots,n \tag{3}$$

The details of developing Eq. (3) are provided in Appendix A. All the terms in Eq. (3), except for the support frictional force $N(t)$, are determined from experimental measurements; the nonlinear normal modes $\omega_i(a), \tilde{\phi}_i(x,a)$ and the support equivalent flexural stiffness $k_\theta(a)$ are identified from experimental results obtained at different vibration levels a, the generalized coordinates $q_i(t)$and their time derivatives are obtained from measured responses and the excitation force $f(t)$ is measured directly. With all these information available, one may employ the force state mapping technique [18,19] to identify the relations between support frictional force $N(t)$ and the states $q(t)$, $\dot{q}(t)$.

Physical interpretation for identified force $N(t)$ is readily available when it is described in terms of $u(t)$, $\dot{u}(t)$defining the relative motion in horizontal direction at the friction support and its time derivative. The relative displacement at the friction support is governed by three different effects included in the right hand side of the following identity:

$$u(t) = -\frac{1}{2}\int_0^L \left(\frac{\partial w(x,t)}{\partial x}\right)^2 dx + r\frac{\partial w(L,t)}{\partial x} + N(t)L/AE \tag{4}$$

The shortening of the beam due to its lateral bending motion is described by the first term on the right hand side of Eq. (4). The second term is the relative motion due to rotation of the beam end, and the last term indicates the axial deformation due to frictional force $N(t)$.

The states $u(t)$, $\dot{u}(t)$are obtained using estimates of $N(t)$ and lateral motion of the beam defined in Eq. (2). In the following, experiments on the beam shown in Fig. 1 are performed and information required to determine the beam nonlinear normal modes and the frictional contact force are recorded.

3. Experimental case study

A uniform steel beam of length L=600 mm, width b=40 mm, and thickness h=5 mm clamped at one end and supported using a frictionally contact interface at the other end is employed in this experimental study. The frictionally contact boundary condition is provided by a pin welded to the beam end and is allowed to slip on a steel block as shown in Fig. 1. The pin has a radius of r=6 mm and its length is equal to the beam width. A constant normal force is applied to the pin using suspended mass blocks. The setup allows for the application of known preloads to the contact interface. The structure is excited using a B&K4200 mini shaker attached through a stinger to the structure at distance S=550 mm from the clamped end. A B&K8200 force transducer is placed between stinger and the structure to measure the excitation force $f(t)$. The structure responses are measured using three accelerometers mounted on the beam at locations x_1=550 mm, x_2=300 mm, and x_3=100 mm (measured from the beam clamped end).

Dynamic responses of the structure are measured while the contact surface is normally loaded with 15 kg mass blocks, i.e. the blocks are equivalent to 147.15 N gravity force. Initially the structure is excited using a low level random force, ensuring the frictional contact interface is in stick regime, and the linear frequency response functions are measured.

Fig. 2 shows the driving point frequency response function recorded a low level of random excitation force. The corresponding natural frequencies are tabulated in Table 1.

The arranged contact interface exhibits different behaviors depending on the vibration amplitude level *a*. In low excitation amplitude levels the interface is in stick regime and behaves linearly. Nonlinear behavior arises due to micro- and macro-slippage as the excitation force level increases. In the following the behavior of contact interface is investigated at different vibration amplitudes.

There are two common approaches in experimentally determining the frequency response curves of a nonlinear structure, namely measuring the FRFs at a constant force level or at a constant response level [23]. In this paper the latter approach is used based on the fact that the nonlinear mechanisms involved in the interface are displacement dependent and keeping the response amplitude level constant insures the nature of these mechanisms do not change in different frequencies. In these experiments the structure is excited using a single harmonic force. The excitation frequency is chosen close to the first resonance frequency of the structure and the force amplitude is tuned such that the accelerations at

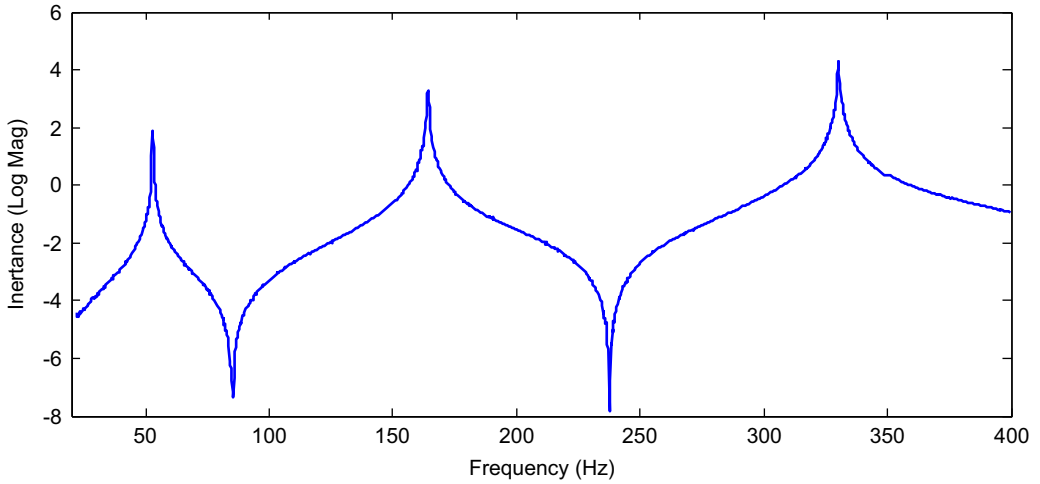

Fig. 2. Driving point frequency responses at low level excitations.

Table 1
Resonance frequencies at low level random excitations (Hz)

ω_1	ω_2	ω_3
52.85	164.00	330.25

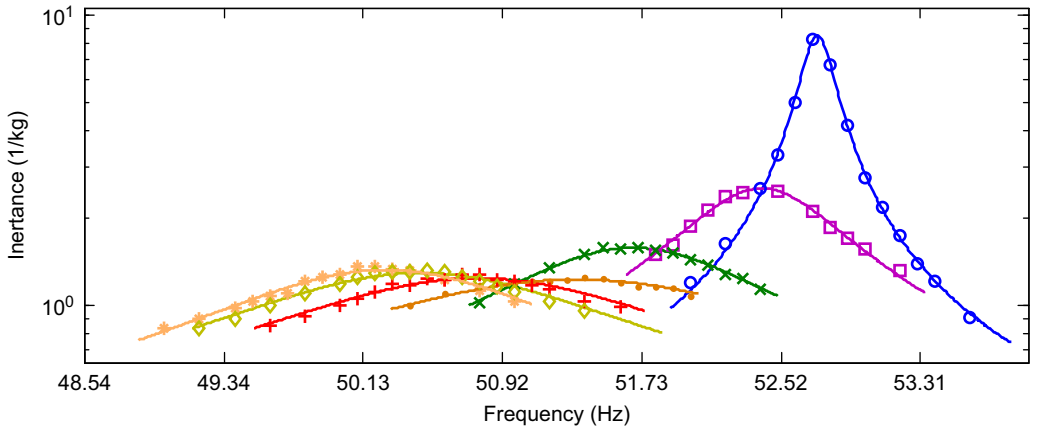

Fig. 3. Measured and fitted frequency responses at response amplitudes of 10 m/s^2(circles), 20 m/s^2(squares), 30 m/s^2(×), 40 m/s^2(points), 50 m/s^2(+), 60 m/s^2(diamonds), and 70 m/s^2(*).

driving point remain constant in the desired frequencies. The force and response signals are recorded and in order to generate the linearized frequency response functions a curve is fitted to the measured data near the resonance points. Bandwidth of selected points in curve fitting around each resonance point is 1 Hz. The selected small bandwidth ensures minimum deviation of response amplitude at each vibration level. Fig. 3 shows the fitted frequency response curves at the driving point in different response amplitudes.

The frequency responses shown in Fig. 3 resemble the equivalent linear behavior of the structure. This is due to the fact that the response amplitude levels are kept constant during measurement of each frequency response. It should be noted that although the resultant frequency responses look like linear FRFs the time domain signals, i.e. measured force and response signals, contain higher harmonics due to nonlinearity effects and can be used for the characterization of the contact interface [24].

The obtained frequency responses reveal changes in peak amplitudes. The resonant frequency shifts to the left, indicating the stiffness softening characteristics of contact interface. The peak amplitude of the measured frequency response function is an indicator of damping in the structure; it initially decreases and then increases. The initial increase in the damping is a direct result of initiation of micro-slips in the contact interface. At higher response levels macro-slips occurs in the interface and damping mechanism is governed by Coulomb friction law. The equivalent linear damping model for the Coulomb friction is proportional to the inverse of the response amplitude, i.e. $c_{eq}=4c/\pi\omega U$, where U is the amplitude of time dependent displacement $u(t)$, and c is the limit friction force. It is evident from the expression of c_{eq} as the amplitude is increasing the equivalent linear damping decreases. In fact by increasing the response amplitude level, the contact interface starts to slip, resulting in decreasing the contact stiffness. The decrease and increase in peak amplitudes of FRFs at different response amplitude levels presented in Fig. 3 is an indicator of the displacement dependent nature of damping characteristic involved in the frictional contact interface. One should note that in general the changes in peak amplitudes may also happen due to the changes in the mode shapes of the structure but this is not the case here.

The observed features of frictionally contact interface, i.e. the softening effects and displacement dependent damping characteristics, are used in constructing a suitable model for the contact interface. In the next section the nonlinear normal modes of structure are identified and the contact shear forces are determined using these experimental observations.

4. Evaluation of the test results

The measured force and acceleration signals are used in this section to reconstruct the nonlinear restoring forces in the contact interface. This reconstruction is performed using Eq. (3) requiring the equivalent stiffness $k_\theta(a)$, the nonlinear normal modes$\omega_i(a)$, $\vec{\phi}_i(x,a)$, and generalized coordinates $\ddot{q}_i(t)$, $q_i(t)$. The first part of this section deals with determination of the beam nonlinear normal modes. Then the measured accelerations and determined nonlinear normal modes are employed to calculate the generalized coordinates using Eq. (2).

The frictional force $N(t)$ produces two separate nonlinear effects in the system: a local symmetrical nonlinearity at the support and a nonsymmetrical global geometrical stiffness in the beam. In reducing the order of model as defined in Eq. (2), one may consider the normal modes of the following system:

$$EI\frac{\partial^4 w}{\partial x^4}+\rho A\frac{\partial^2 w}{\partial t^2}=0 \tag{5}$$

$$w(0,t)=0,\quad \frac{\partial w(0,t)}{\partial x}=0,\quad w(L,t)=0,\quad EI\frac{\partial^2 w(L,t)}{\partial x^2}=k_\theta(a)\frac{\partial w(L,t)}{\partial x} \tag{6}$$

The flexural spring $k_\theta(a)$ is the equivalent stiffness of the frictional support at each vibration amplitude level. The model defined in Eqs. (5) and (6) ignores the geometrical stiffness induced in the beam due to frictional forces at the support. However one only employs this model in estimating the amplitude dependent nonlinear normal modes to reduce the order of model defined in Eq. (1) and the geometric stiffness effects are not ignored in the identification procedure.

Szemplinska-Stupnicka [21,22] showed that the deformed shape of system in resonant conditions can be considered a good approximation of the nonlinear normal mode; this concept is used in the present work to extract the nonlinear normal mode. The definition of nonlinear normal mode employed in this research work is appropriate for structures with well separated modes and no coupling effects between the modes.

The structure has well separated modes and the non-proportional damping induced by the frictional contact has little influence in creating complex valued modes; the mode shapes remain almost real. The mode shapes obtained from the classical Euler–Bernoulli beam theory and boundary conditions defined in Eqs. (5) and (6) are used to construct the nonlinear normal modes of the system under consideration at different vibration amplitudes a.

In the measurements, the frequency responses near the first resonance frequency are recorded at different amplitudes. Using these measured responses one may identify the first natural frequency of the corresponding linear system. The natural frequencies are identified by curve fitting each frequency response and identifying the resonance frequency. The amplitude dependent resonance frequencies obtained from the measurements are tabulated in Table 2. In this table the corresponding nonlinear flexural spring $k_\theta(a)$ are also shown. The stiffness $k_\theta(a)$ at each amplitude a is identified by solving the characteristic equation of linear problem defined in Eqs. (5) and (6). In development of the characteristic equation, the beam is divided into four parts: the first part spans between fixed end and the accelerometer three

Table 2
Changes of 1st natural frequency and the support stiffness with respect to the vibration amplitude

a (m/s^2)	$\omega_1(a)$ (Hz)	$k_\theta(a)$ (kN m/rad)
Linear	52.85	197.4
10	52.79	192.8
20	52.30	167.1
30	51.62	125.4
40	50.63	73.6
50	50.55	71.4
60	50.30	65.7
70	50.11	58.7

at x_3, parts two and three are located between the three accelerometers, and part four is located between driving point and frictional support. The characteristic equation of the system is developed by considering the boundary conditions and the compatibility requirements at the interface of each of the two parts. In deriving the compatibility equations it is assumed the slopes and displacements at the interface of each two parts are continuous but the shear forces and bending moments abruptly change due to mass and inertia effects of the accelerometers and the force transducer.

The amplitude dependent nonlinear normal modes $\omega_i(a)$, $\tilde{\phi}_i(x,a)$ are evaluated at different response amplitudes a by solving the eigenproblem defined in Eqs. (5) and (6) and adopting corresponding support flexural stiffness $k_\theta(a)$ tabulated in Table 2.

In the following, calculations of the generalized coordinates are described. One may employ Eq. (2) and define a direct relation between measured acceleration signals and corresponding values in the generalized coordinates. The number of nonlinear normal mode shapes used in Eq. (2) may not exceed the number of independently measured vibration signals. In this paper it is initially assumed only the first three normal modes contribute to the dynamic response of the beam as the structure has well separated modes and only three accelerometers are employed in the measurement setup. The validity of this assumption will be verified by observing the response is dominated only by the first two modes.

It is possible to calculate the generalized acceleration vector using the measured accelerations at j points, $j \geq n$, and the mode shape matrix as

$$\ddot{\mathbf{q}}(\mathbf{t}) = \begin{Bmatrix} \ddot{q}_1(t) \\ \ddot{q}_2(t) \\ \vdots \\ \ddot{q}_n(t) \end{Bmatrix} = \begin{bmatrix} \tilde{\phi}_1(a,x_1) & \tilde{\phi}_2(a,x_1) & \cdots & \tilde{\phi}_n(a,x_1) \\ \tilde{\phi}_1(a,x_2) & \tilde{\phi}_2(a,x_2) & \cdots & \tilde{\phi}_n(a,x_2) \\ \vdots & \vdots & \ddots & \vdots \\ \tilde{\phi}_1(a,x_j) & \tilde{\phi}_2(a,x_j) & \cdots & \tilde{\phi}_n(a,x_j) \end{bmatrix}^+ \begin{Bmatrix} \ddot{w}(x_1,t) \\ \ddot{w}(x_2,t) \\ \vdots \\ \ddot{w}(x_j,t) \end{Bmatrix} = \mathbf{\Phi}^+ \ddot{\mathbf{w}} \tag{7}$$

The superscript $()^+$ refers to pseudo-inverse of the matrix. Reconstruction of $N(t)$ using force-state mapping requires the knowledge of $\mathbf{q}(\mathbf{t})$, which is obtained by time integration of $\ddot{\mathbf{q}}(\mathbf{t})$ twice. As the excitation force in the experiments is simple harmonic, it is possible to perform the integrations analytically. The response contains the same harmonic as the excitation force and its multiples due to nonlinear effects in the structure. Considering the excitation frequency is ω, a Fourier series of the following form can be fitted to every measured acceleration signal:

$$\ddot{q}_i(t) = \sum_{m=1}^{M} (A_m \cos(m\omega t) + B_m \sin(m\omega t)), \quad i = 1,2,3 \tag{8}$$

where the coefficients A_m and B_m are obtained from data fitting (see [25] for more details). In this study the number of harmonics required to match the measured data is found to be $M=5$. The vector $q(t)$ is obtained by time integrating $\ddot{q}(t)$ twice as

$$q_i(t) = A_0 - \sum_{m=1}^{M} \left(\frac{A_m}{(m\omega)^2} \cos(m\omega t) + \frac{B_m}{(m\omega)^2} \sin(m\omega t) \right), \quad i = 1,2,3 \tag{9}$$

Fig. 4 shows the generalized coordinates $q(t)$ obtained from Eq. (9) at $a=70$ m/s^2. At this amplitude we expect higher modes to have the highest contributions in the response compared to other vibration amplitudes. As it can be seen in Fig. 4 the response is dominated by the first mode contribution, the effect of second mode in response is marginal, and the third mode contribution in the response is zero. The response at the driving point is reconstructed using only the first two modes and is compared with the measured accelerations in Fig. 5. There is an excellent agreement between the measured and predicted responses ensuring the accuracy of calculated generalized accelerations.

At this point all prerequisites for calculation of nonlinear restoring force $N(t)$ using force state mapping are available. The restoring force is constructed in the next section and a predictive model for this force at the support interface is identified.

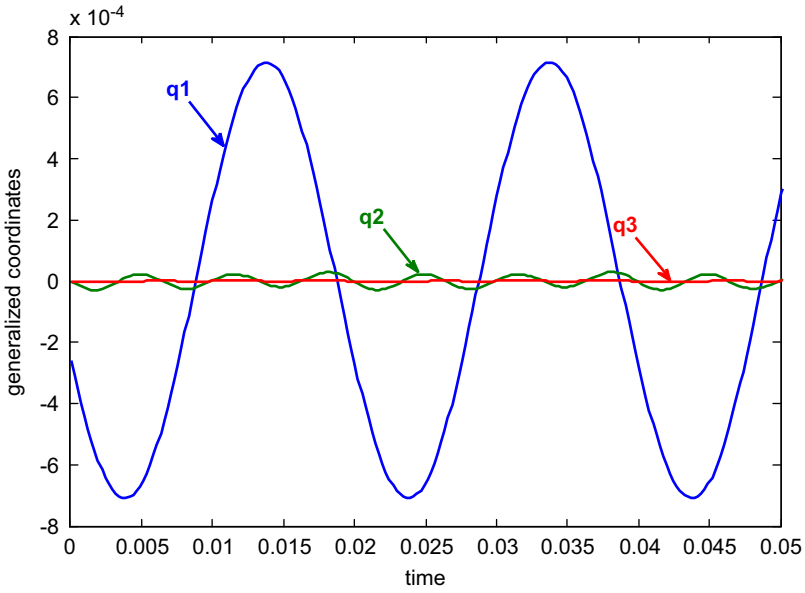

Fig. 4. The generalized coordinates at a=70 m/s^2.

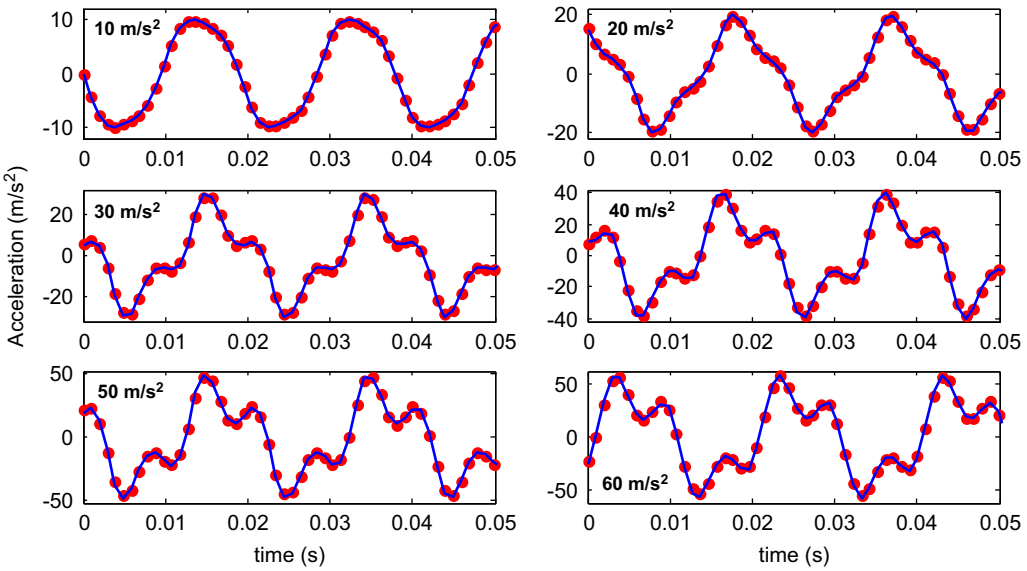

Fig. 5. Accelerations at the driving point, measured (solid line) and reconstructed (circles).

5. Identification of restoring forces

In order to reconstruct the frictional force $N(t)$ one may start from Eq. (3) and evaluate the frictional force using the first two generalized coordinates; it is shown in Fig. 4 only these two modes contribute to time response. The frictional force is expanded using Fourier series in time domain up to the fifth harmonic of the excitation force as these harmonics appear in the generalized coordinates $q_1(t)$ and $q_2(t)$. Then the coefficients of the Fourier series are obtained by harmonic balancing of Eq. (3) when i is set to 1 and 2.

Having obtained the frictional force $N(t)$, one may determine the deformation $u(t)$ at the frictional support using Eq. (4). Its time derivative $\dot{u}(t)$ is obtained by using the periodic property of $u(t)$ consisting of few harmonics and the differentiation is performed in the frequency domain. Calculations of $u(t)$ and $\dot{u}(t)$ allow one to draw the three dimensional plot of hysteresis loops, i.e. frictional force N(t) vs. u(t) and $\dot{u}(t)$. The results are shown in Figs. 6–8.

It is observed the identified hysteresis loops of the frictional support are similar to those predicted by the constitutive elasto-plastic Valanis model and this predictive model is capable of simulating the nonlinear characteristics of the contact.

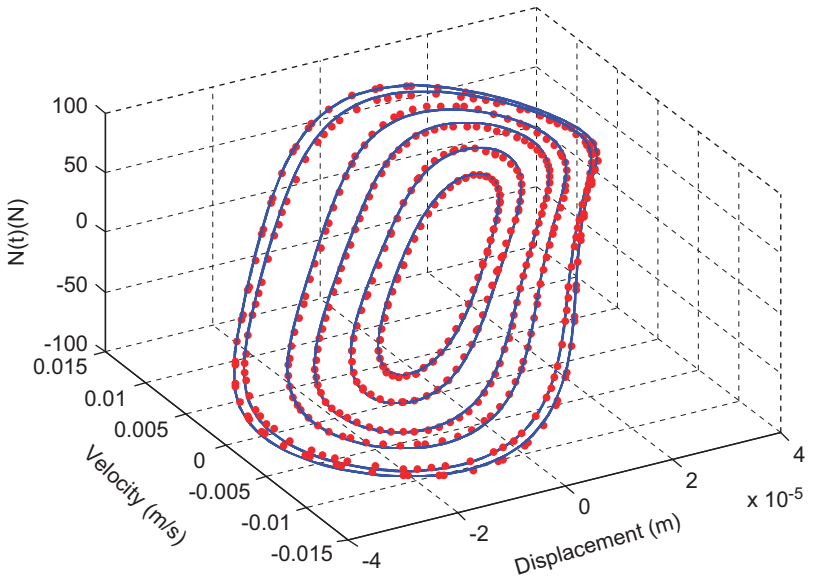

Fig. 6. The force-state map of the frictional force within measurement range of 20 m/s^2 (inner loop) to 70 m/s^2 (outer loop): measured (circles) and predicted (solid line).

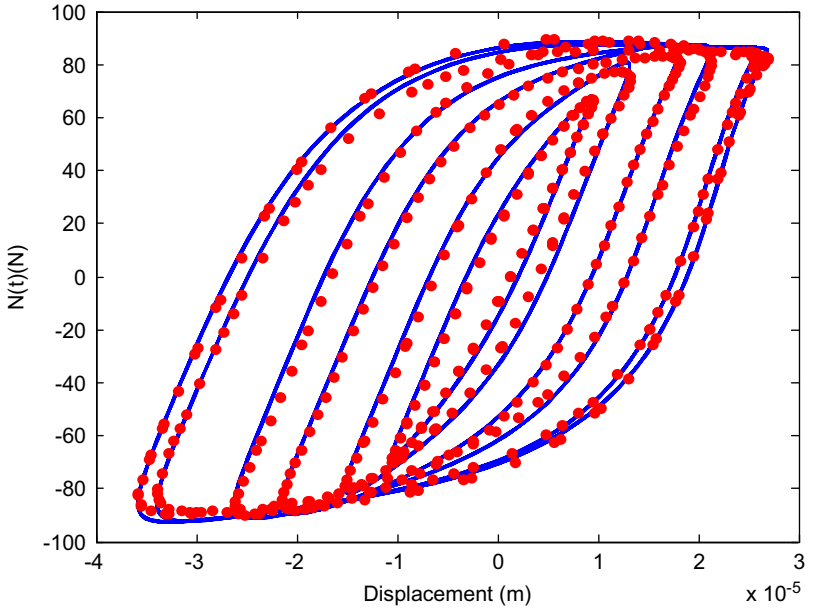

Fig. 7. The hysteresis loops $N(t)$ vs. $u(t)$ within measurement range of 20 m/s^2 (inner loop) to 70 m/s^2 (outer loop): measured (circles) and predicted (solid line).

Introduction of this predictive model with appropriate parameters enables one to determine the frictional forces at vibration levels other than those employed in the identification of the contact model parameters.

The Valanis predictive model for the boundary contact interface is adopted by setting the contact parameters such that it produces consistent results with those observed in force-state maps, i.e. Figs. 6–8. The Valanis elasto-plastic constitutive model relates the rate of change in frictional forces N(t) to u(t) and $\dot{u}(t)$ as follows:

$$\dot{N}(t)=\frac{e_0\dot{u}\left[1+\frac{\lambda}{e_0}\mathrm{sgn}(\dot{u})(e_t u-N(t))\right]}{1+\kappa\frac{\lambda}{e_0}\mathrm{sgn}(\dot{u})(e_t u-N(t))},\quad \lambda=\frac{e_0}{\alpha_0\left(1-\kappa\frac{e_t}{e_0}\right)} \tag{10}$$

The model parameters are: e_0 contact shear stiffness in stick, e_t contact shear stiffness in macro-slip, κ is a control parameter to define a smooth transition from stiction to the macro-slip due to micro-slips in the contact interface, and

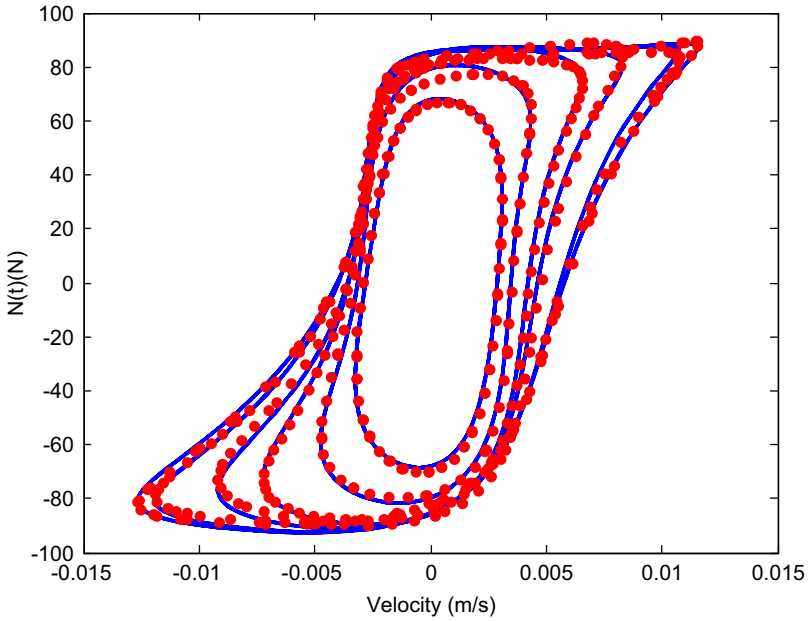

Fig. 8. The hysteresis loops $N(t)$ vs. $\dot{u}(t)$ within measurement range of 20 m/s^2 (inner loop) to 70 m/s^2 (outer loop): measured (circles) and predicted (solid line).

Table 3
The identified parameters for Valanis model at a=70 m/s^2

Parameter	Value
e_0 (N/m)	7.9e6
e_t (N/m)	$\approx$ 0.0
κ	0.3
λ (1/m)	8.7e4

α_0 sets the yield point in the contact interface hysteresis loop. A complete description of the contact model is provided in Ref. [11]. These parameters have clear physical meanings and can be directly extracted from the identified hysteresis loops of Figs. 6–8 with minimum computational efforts. The selected predictive model is capable of taking into account the dependency of N(t) to its previous states, which is a distinct property of friction phenomenon.

Identification of frictional model parameters e_0, e_t, κ and λ is performed by fitting the hysteresis loop of N(t) vs. u(t) from the measurements obtained at a constant level of vibration a=70 m/s^2. This results in a set of parameters as tabulated in Table 3.

Fig. 8 compares the hysteresis loops N(t) vs. u(t) obtained from experimental results with those predicted using the identified Valanis model at different vibration levels. The model predictions show good agreement with experimental observations; the set of parameters obtained at a=70 m/s^2 predicts the support interface behavior at all other vibration levels accurately. The dependency of N(t) to $\dot{u}(t)$ is shown in Fig. 8 and again there is a good agreement between the identified model predictions and the observed behavior of the frictional support.

The agreement between experimentally obtained frictional forces at the support and the contact interface model predictions at vibration levels from which measured data are not used in the identification procedure shows the validity and accuracy of the procedure adopted in reconstructing the nonlinear contact interface model. It also indicates the identified model capability in representing the physical mechanisms involved in frictional support, which is an important issue in employing the model in loading conditions other than those it is subjected in the experimental measurements.

In the present case study a structure with weak local nonlinearity is excited using a single harmonic force near its first resonance frequency and the response is dominated by the first nonlinear mode. If the excitation type and/or contact mechanisms are changed the overall strategy to identify the restoring forces remains the same but the number of nonlinear modes participating in the series expansion of response would certainly change. The key to successful identification of contact restoring forces in the proposed method of this paper is the way nonlinear modes are defined. The frictional contact under consideration in this paper is displacement dependent within the considered range of vibrations and the defined nonlinear modes are capable of reproducing the deformed shape of the harmonically excited structure. In other cases with more general loading conditions and/or complicated contact mechanism one may employ a more general definition for nonlinear normal modes as a twodimensional invariant manifold in phase space presented by Shaw and Pierre [26].

6. Conclusion

Dynamic characteristics of a beam with frictional contact support are investigated. The contact interface is subject to a constant normal load and the system frequency responses are recorded at constant vibration levels. The contact frictional shear force is identified by expanding the beam response using its nonlinear normal modes. These nonlinear normal modes are identified from the experimentally recorded data and the behavior of the system is accurately expressed using only the first two nonlinear modes. The reduced order model of the system developed using the nonlinear normal modes predicts the experimental observations accurately and provides the required means to represent the support frictional force in terms of its states, i.e. the contact shear deformation and its time derivative. The force state map of the support friction force is generated to identify a predictive model for contact shear force. The selected contact interface constitutive law is based on the Valanis elasto-plastic concept and contact parameters are identified using the force state map of only one measured vibration level. The identified contact interface model is capable of accurately regenerating frictional forces at all other measured vibration levels, indicating the validity of the identified model in representing the physical mechanism of the frictional support.

Appendix A

This section describes the process of discretizing the beam equation of motion. Projecting the governing equation (1) onto nonlinear normal modes one arrives at the following:

$$\int_0^L \tilde{\phi}_i(x,a)\left(EI\frac{\partial^4 w}{\partial x^4}-N(t)\frac{\partial^2 w}{\partial x^2}+\rho A\frac{\partial^2 w}{\partial t^2}-f(t)\delta(x-S)+rN(t)\delta'(x-L)\right)dx=0 \tag{A1}$$

The bending moment caused by friction at the equation of motion is treated as an external force therefore the beam boundary conditions are fixed-simply supported:

$$w(0,t)=0,\quad \frac{\partial w(0,t)}{\partial x}=0,\quad w(L,t)=0,\quad \frac{\partial^2 w(0,t)}{\partial x^2}=0 \tag{A2}$$

The nonlinear normal modes satisfy the geometrical boundary conditions:

$$\tilde{\phi}_i(0,a)=0,\quad \tilde{\phi}_i(L,a)=0,\quad \frac{\partial\tilde{\phi}_i(0,a)}{\partial x}=0,\quad i=1,2,\ldots,n \tag{A3}$$

Employing Eqs. (A2) and (A3) in integration by parts of the integral defined in Eq. (A1) one obtains

$$EI\int_0^L \frac{\partial^2\tilde{\phi}_i(x,a)}{\partial x^2}\frac{\partial^2 w}{\partial x^2}\,dx-N(t)\int_0^L \frac{\partial\tilde{\phi}_i(x,a)}{\partial x}\frac{\partial w}{\partial x}\,dx+\int_0^L \tilde{\phi}_i(x,a)\rho A\frac{\partial^2 w}{\partial t^2}\,dx\quad -f(t)\tilde{\phi}_i(S,a)-rN(t)\frac{\partial\tilde{\phi}_i(L,a)}{\partial x}=0 \tag{A4}$$

Expanding the beam motion using the nonlinear normal modes as defined in Eq. (2) leads to

$$\begin{aligned}&EI\sum_{r=1}^n q_r(t)\int_0^L \frac{\partial^2\tilde{\phi}_i(x,a)}{\partial x^2}\frac{\partial^2\tilde{\phi}_r(x,a)}{\partial x^2}\,dx+\sum_{r=1}^n \frac{\partial^2 q_r(t)}{\partial t^2}\int_0^L \rho A\tilde{\phi}_i(x,a)\tilde{\phi}_r(x,a)\,dx\\&+N(t)\sum_{r=1}^n q_r(t)\int_0^L \frac{\partial\tilde{\phi}_i(x,a)}{\partial x}\frac{\partial\tilde{\phi}_r(x,a)}{\partial x}\,dx-f(t)\tilde{\phi}_i(S,a)-rN(t)\frac{\partial\tilde{\phi}_i(L,a)}{\partial x}=0\end{aligned} \tag{A5}$$

Eq. (A5) can be converted to the classical form of equation of motion in the modal domain by further simplifications. Considering the first two terms of Eq. (A5) one may rewrite them as

$$\begin{aligned}&EI\sum_{r=1}^n q_r(t)\int_0^L \frac{\partial^2\tilde{\phi}_i(x,a)}{\partial x^2}\frac{\partial^2\tilde{\phi}_r(x,a)}{\partial x^2}\,dx+\sum_{r=1}^n \frac{\partial^2 q_r(t)}{\partial t^2}\int_0^L \rho A\tilde{\phi}_i(x,a)\tilde{\phi}_r(x,a)\,dx\\&\quad=\left(EI\sum_{r=1}^n q_r(t)\int_0^L \frac{\partial^2\tilde{\phi}_i(x,a)}{\partial x^2}\frac{\partial^2\tilde{\phi}_r(x,a)}{\partial x^2}\,dx+k_\theta(a)\frac{\partial\tilde{\phi}_i(L,a)}{\partial x}\sum_{r=1}^n q_r(t)\frac{\partial\tilde{\phi}_r(L,a)}{\partial x}\right)\\&\quad+\sum_{r=1}^n \frac{\partial^2 q_r(t)}{\partial t^2}\int_0^L \rho A\tilde{\phi}_i(x,a)\tilde{\phi}_r(x,a)\,dx-k_\theta(a)\frac{\partial\tilde{\phi}_i(L,a)}{\partial x}\sum_{r=1}^n q_r(t)\frac{\partial\tilde{\phi}_r(L,a)}{\partial x}\end{aligned} \tag{A6}$$

Employing the linearized beam modal orthogonality relations:

$$\int_0^L EI\frac{\partial^2\tilde{\phi}_i(x,a)}{\partial x^2}\frac{\partial^2\tilde{\phi}_r(x,a)}{\partial x^2}\,dx+k_\theta(a)\frac{\partial\tilde{\phi}_i(L,a)}{\partial x}\frac{\partial\tilde{\phi}_r(L,a)}{\partial x}=\omega_i{}^2\delta_{ir} \tag{A7}$$

$$\int_0^L \rho A\tilde{\phi}_i(x,a)\tilde{\phi}_r(x,a)\,dx=\delta_{ir} \tag{A8}$$

In Eq. (A6) one establishes.

References

[1] J.P. Den Hartog, Forced vibrations with combined Coulomb and viscous friction, Transactions of the ASME: Applied Mechanics 53 (9) (1931) 107–115.
[2] E.H. Dowell, Damping in beams and plates due to slipping at the support boundaries, Journal of Sound and Vibration 105 (2) (1986) 243–253.
[3] Y. Lee, Z.C. Feng, Dynamic responses to sinusoidal excitations of beams with frictional joints, Communications in Nonlinear Science and Numerical Simulation 9 (2004) 571–581.
[4] A.A. Ferri, A.C. Bindemann, Damping and vibration of beams with various types of frictional support conditions, ASME Journal of Vibration and Acoustics 114 (1992) 289–296.
[5] A.A. Ferri, Friction damping and isolation systems, Journal of Mechanical Design 117 (1995) 196–206.
[6] E.J. Berger, Friction modeling for dynamic system simulation, Applied Mechanics Reviews 55 (6) (2002) 535–577.
[7] R.A. Ibrahim, C.L. Pettit, Uncertainties and dynamic problems of bolted joints and other fasteners, Journal of Sound and Vibration 279 (3–5) (2005) 857–936.
[8] W.D. Iwan, A distributed-element model for hysteresis and its steady-state dynamic response, ASME Journal of Applied Mechanics 33 (1966) 893–900.
[9] P.R. Dahl, Solid friction damping of mechanical vibrations, AIAA Journal 14 (1976) 1675–1682.
[10] K.C. Valanis, A theory of viscoplasticity without a yield surface, Archives of Mechanics 23 (4) (1971) 171–191.
[11] L. Gaul, J. Lenz, Nonlinear dynamics of structures assembled by bolted joints, Acta Mechanica 125 (1997) 169–181.
[12] J. Swevers, F. Al-Bender, C.G. Ganesman, T. Prajogo, An integrated friction model structure with improved presliding behavior for accurate friction compensation, IEEE Transactions on Automatic Control 45 (4) (2002) 675–686.
[13] V. Lampaert, J. Swevers, F. Al-Bender, Modification of the Leuven integrated friction model structure, IEEE Transactions on Automatic Control 47 (4) (2002) 683–687.
[14] D.A. Haessig Jr., B. Friedland, On the modeling and simulation of friction, ASME Journal of Dynamic Systems, Measurement, and Control 113 (1991) 354–362.
[15] C. Canudas de Wit, H. Olsson, K.J. Astrom, P. Lischinsky, A new model for control of systems with friction, IEEE Transactions on Automantic Control 40 (3) (1995) 419–425.
[16] L. Gaul, R. Nitsche, The role of friction in mechanical joints, Applied Mechanics Reviews 52 (2) (2001) 93–106.
[17] D.J. Segalman, Modeling joint friction in structural dynamics, Structural Control Health Monitoring 13 (2006) 430–453.
[18] S.F. Masri, T.K. Caughey, A nonparametric identification technique for nonlinear dynamic problems, Journal of Applied Mechanics 46 (1979) 433–447.
[19] E.F. Crawley, A.C. Aubert, Identification of nonlinear structural elements by force-state mapping, AIAA Journal 24 (1) (1986) 155–162.
[20] L. Meirovitch, in: Principles and Techniques of Vibrations, Prentice-Hall, Inc., Upper Saddle River, NJ, 1997.
[21] W. Szemplinska-Stupnicka, The modified single mode method in the investigations of the resonant vibrations of nonlinear systems, Journal of Sound and Vibration 65 (1979) 475–489.
[22] W. Szemplinska-Stupnicka, Nonlinear normal modes and generalized Ritz method in the problems of vibrations of nonlinear elastic continuous systems, International Journal of Non-Linear Mechanics 18 (1983) 149–165.
[23] S. Perinpanayagam, D. Robb, D. J. Ewins, J. Moreno Barragan, Non-linearities in an aero-engine structure: from test to design, in: Proceedings of the 2005 International Conference on Modal Analysis, Noise and Vibration Engineering, Leuven, Belgium, 2004, pp. 3167–3182.
[24] A. Vakakis, D.J. Ewins, Effects of weak nonlinearities on modal analysis, Mechanical System and Signal Processing 8 (2) (1994) 175–198.
[25] K. Worden, G.R. Tomlinson, in: Nonlinearity in Structural Dynamics: Detection, Identification and Modeling, Institute of Physics Publishing, Bristol and Philadelphia, 2001.
[26] S.W. Shaw, C. Pierre, Nonlinear normal modes and invariant manifolds, Journal of Sound and Vibration 150 (1991) 170–173.